

Cross-extrapolation reconstruction of low-rank functions and application to quantum many-body observables in the strong coupling regime

Matthieu Jeannin,^{1,*} Yuriel Núñez-Fernández,² Thomas Kloss,² Olivier Parcollet,^{3,4} and Xavier Waintal^{1,†}

¹Univ. Grenoble Alpes, CEA, Grenoble INP, IRIG, Pheligs, F-38000 Grenoble, France

²Univ. Grenoble Alpes, CNRS, Institut Néel, 38000 Grenoble, France

³Center for Computational Quantum Physics, Flatiron Institute, 162 5th Avenue, New York, NY 10010, USA

⁴Université Paris-Saclay, CNRS, CEA, Institut de physique théorique, 91191, Gif-sur-Yvette, France

(Dated: January 12, 2024)

We present a general-purpose algorithm to extrapolate a low rank function of two variables from a small domain to a larger one. It is based on the cross-interpolation formula. We apply it to reconstruct physical quantities in some quantum many-body perturbative expansions in the real time Keldysh formalism, considered as a function of time t and interaction U . These functions are of remarkably low rank. This property, combined with the convergence of the perturbative expansion in U both at finite t (for any U), and small U (for any t), is sufficient for our algorithm to reconstruct the physical quantity at long time, strong coupling regime. Our method constitutes an alternative to standard resummation techniques in perturbative methods, such as diagrammatic Quantum Monte Carlo. We benchmark it on the single impurity Anderson model and show that it is successful even in some regime where standard conformal mapping resummation techniques fail.

I. INTRODUCTION

Many important problems in physics could formally be solved by extrapolating from a regime of parameters where physical quantities are known with a high degree of precision to a more challenging regime. Common examples include extrapolating from weak to strong coupling, from large to small temperature or from short to long times. Nevertheless, extrapolation is a notoriously difficult problem to control, unless it is based on some underlying rigid mathematical structure that strongly constraints the extrapolation. Such a structure could take various form such as an analytical structure in the complex plane [1, 2], semi-positive definiteness [3] or in the case of the present article, the low-rankness of some function. The approach that we will follow below is to control the extrapolation with - not just one but - two different variables.

Important extrapolation problems in computational quantum many-body physics arise in the context of perturbative series expansions in power of the interaction. The challenge is to resum them in strongly interacting regimes, i.e. beyond the *perturbative regime* defined as the range of small interactions where the series actually converges. Several methods have been used in the literature to do this, such as conformal mappings in the complex interaction plane [1, 4–7] Padé methods [2, 8, 9], or other mathematical approaches [10–16]. Recently, several remarkable results have been obtained by combining these ideas with numerical methods to compute the series to relatively large orders, both in equilibrium with diagrammatic quantum Monte Carlo (QMC) [17–19] and out of equilibrium [5, 20]. Let us mention for example an exact solution of a simple quantum dot model, in the

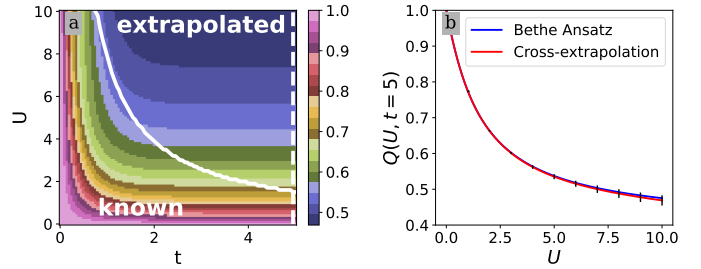


Figure 1. Example of Cross-extrapolation. (a) Charge $Q(U, t)$ in the Anderson impurity model, at temperature $T = 0$. U is the interaction, t the time after switching of the interaction. The charge can be computed on the region below the white line (using an expansion in power of U to order 22); the region above the white line shows the double time-interaction cross-extrapolation. (b) Comparison between the extrapolation at $t = 5$ [along the dash line shown in (a)] and the exact result (known from Bethe Ansatz).

long time out of equilibrium steady state or in the Kondo regime [1, 2, 5, 20–22], and an exact solution of the Hubbard model in a pseudo gap regime [23, 24]. Nevertheless, despite their numerous successes, these approaches have limitations and are difficult to automatize, for example in the context of quantum embedding solvers. For instance, the singularities of the physical quantities in the complex plane of the interaction U can limit our ability to use conformal mappings.

In this paper, we follow a different route to reach the strong coupling regime. We consider a physical quantity $Q(U, t)$ that can be computed precisely for large t if U is sufficiently small *and* for relatively large U if t is small enough. Here U is the interaction strength and t the time after an initial quench of the interaction. Two kind of extrapolations could be attempted: as a function of U (for given t) or as a function of t (for given U). Our “cross-extrapolation” algorithm performs both extrapolations

* matt.jeannin@gmail.com

† xavier.waintal@cea.fr

simultaneously, using the assumption that $Q(U, t)$ is low rank [i.e. well approximated by a sum of a few terms of the form $f(t)g(U)$]. We shall show that this assumption is verified in concrete examples. Furthermore, this low-rank structure is sufficient to reconstruct the physical quantities at large interactions and long times, based only on its value in the perturbative regime. Let us mention that a different form of "low rankness" (using the quantics representation) has been exploited recently in a - one variable - extrapolation scheme [25] to go beyond linear predictions. Both this scheme and ours could possibly be combined (see [26] for a link between quantics and cross interpolation).

From a mathematical point of view, the problem is quite general and can be formulated as follows. Given a function which is low-rank in some rectangular domain (as defined precisely in Sect. II), how to reconstruct it from its values in a subdomain? In Sect. II, we discuss a simple *cross-extrapolation* algorithm to solve this problem, based on the cross-interpolation (CI) decomposition of a matrix. The algorithm is rank-revealing, i.e. it is able to reconstruct the function but explicitly fails if the function is not of low rank.

Our main result is illustrated in Fig. 1, which shows the charge of a quantum dot in the Anderson impurity model in equilibrium, as a function of U and t . The perturbative series is converged after 22 orders only below the white line. The low-rank extrapolation from this perturbative regime to long times and large interactions is in excellent agreement at equilibrium with Bethe Ansatz benchmarks (Fig. 1b). Furthermore, the underlying property that permits the extrapolation (low-rankness) is very different from the one used in conformal mapping method (positions of the poles and branch cuts in the complex U plane [1, 5]). We explicitly exhibit an example where the former works while the latter fail due to singularities located close to the positive real axis in the complex U plane.

This paper is organized as follows. In Sect. II, we first present the cross-extrapolation algorithm and illustrate it on a simple toy function; in section III, we apply this technique first to the charge of a quantum dot in equilibrium as a benchmark, and then to the current flowing through the dot upon applying a bias voltage; finally we conclude in section IV.

II. CROSS EXTRAPOLATION

In this section, we present our *cross-extrapolation* algorithm and test it on a simple toy function. The problem is the following: given a function $f(x, y)$ defined on domain $\mathcal{D} = [0, l_x] \times [0, l_y]$ but that is known only in a small subdomain $\mathcal{D}_{\text{sub}} \subset \mathcal{D}$ (for instance for $xy < c$), we would like to extrapolate it to its entire domain \mathcal{D} .

The extrapolation scheme requires the function to have a low-rank. More precisely, f is of ϵ -rank χ (i.e. of rank χ up an error ϵ) if a set of χ one dimensional functions

g_k and h_k can be found such that

$$|f(x, y) - \sum_{k=1}^{\chi} g_k(x)h_k(y)| < \epsilon \quad (1)$$

for all x, y . A function is of ϵ -rank $\chi = 1$ if it is almost factorizable. This definition is the direct extension of the same concept for matrices. If we use a discretization grid (x_i, y_j) on the domain, with a step δ ($|x_{i+1} - x_i| < \delta$) then the matrix $M_{ij} = f(x_i, y_j)$ is of ϵ -rank χ . Conversely, if the matrix $M_{ij} = f(x_i, y_j)$ remains of ϵ -rank χ in the continuous limit $\delta \rightarrow 0$ then the function f is of ϵ -rank χ . We will explicitly checked in our applications that the result did not depend on the size of the grid used in the practical discretization.

A. Matrix cross interpolation

Cross-extrapolation is based on the *cross-interpolation* formula for matrices that we briefly recall [27–32]. Given a matrix M_{ij} , we select a set of χ linearly independent lines of indices i_α ($\alpha \in \{1 \dots \chi\}$), and χ linearly independent columns of indices j_β ($\beta \in \{1 \dots \chi\}$). The $\chi \times \chi$ matrix formed by these two sets $P_{\alpha\beta} \equiv M_{i_\alpha, j_\beta}$ is called the pivot matrix. The cross-interpolation M^{CI} of M is defined as,

$$M_{ij}^{\text{CI}} \equiv \sum_{\alpha, \beta} M_{i, j_\beta} (P^{-1})_{\beta\alpha} M_{i_\alpha, j} \quad (2)$$

Equation (2) has two main properties [20]: (i) It is an interpolation, i.e. $M_{ij} = M_{ij}^{\text{CI}}$ on the selected lines and columns ($i = i_\alpha$ or $j = j_\beta$); (ii) if M is exactly of rank χ , the approximation is exact: $M = M^{\text{CI}}$. For a ϵ -rank χ matrix, the cross-interpolation formula provides a practical way to obtain its low rank approximation. Crucially, the cross-interpolation is built purely from a few rows and columns of the initial matrix. It *does not* require the knowledge of the entire matrix. This is a sharp contrast with a standard way of constructing a low rank approximation of a matrix, the singular value decomposition (SVD). It can be shown [33–35] that the optimal choice of the rows (i_α) and columns (j_β) corresponds to the maximization of the determinant $|P|$ of the pivot matrix. In practice, the pivot selection is done using efficient heuristics that are much cheaper computationally [29, 36–38]. A standard choice is to build the approximation iteratively by looking for a pivot (i_*, j_*) that currently holds a large error. This new pivot is added to the pivot list ($i_{\chi+1} = i_*$, $j_{\chi+1} = j_*$) to increase $\chi \rightarrow \chi + 1$, see Fig. 11 in Appendix A for an illustration.

Cross-interpolation extends naturally to functions of two variables $f(x, y)$ [29, 37, 39]. Selecting χ pivots (x_α, y_α) and defining the pivot matrix as $P_{\alpha\beta} \equiv f(x_\alpha, y_\beta)$, we approximate $f(x, y) \approx f_\chi^{\text{CI}}(x, y)$ with its cross-interpolation approximation $f_\chi^{\text{CI}}(x, y)$,

$$f_\chi^{\text{CI}}(x, y) \equiv \sum_{\alpha, \beta} f(x, y_\beta) (P^{-1})_{\beta\alpha} f(x_\alpha, y) \quad (3)$$

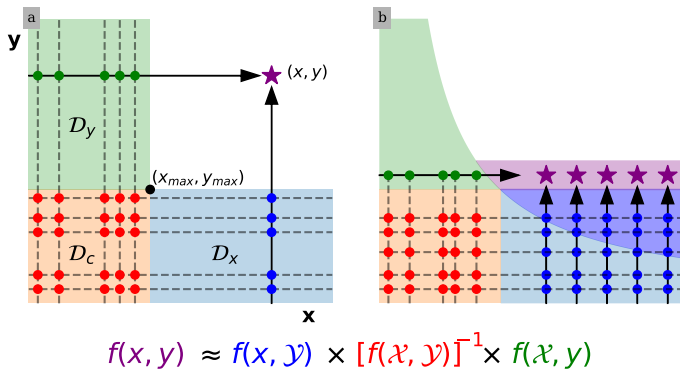


Figure 2. Schematic of the cross-extrapolation algorithm. (a) L -shape subdomain, cf text. The function is known in the colored regions, and the goal is to reconstruct it in the white region, e.g. at the (x, y) represented by the purple star. Red circles correspond to the pivot matrix, blue and green ones to the column and the line of the target value. (b) Hyperbolic subdomain. Each new line (purple) is extrapolated using information available (green, red and light blue) as well as the values newly extrapolated (deep blue) from the previous lines.

This formula is often written using a slice notations (inspired by MATLAB notations): noting \mathcal{X} the list of pivot rows $\{i_1 \dots i_\chi\}$ and \mathcal{Y} the list of pivot columns $\{j_1 \dots j_\chi\}$, one writes

$$f_\chi^{\text{CI}}(x, y) \equiv f(x, \mathcal{Y})f(\mathcal{X}, \mathcal{Y})^{-1}f(\mathcal{X}, y) \quad (4)$$

The principle of the cross-extrapolation is very simple: we will extrapolate $f(x, y)$ using $f_\chi^{\text{CI}}(x, y)$ where the pivots (x_α, y_β) are chosen inside the region \mathcal{D}_{sub} where $f(x, y)$ can be calculated. Property (ii) of the cross-interpolation guarantees that this extrapolation is exact if f is exactly of rank χ and is known with infinite precision.

B. Cross-extrapolation algorithm

1. L -shaped subdomain

We first consider the simple situation where the function is known on a domain that has a L -shape (see Fig. 2). The domain is made of three parts $\mathcal{D}_{\text{sub}} = \mathcal{D}_c \cup \mathcal{D}_x \cup \mathcal{D}_y$ where $\mathcal{D}_c = [0, x_{\text{max}}] \times [0, y_{\text{max}}]$ (represented in orange in Fig. 2), $\mathcal{D}_x = [0, l_x] \times [0, y_{\text{max}}]$ (represented in blue) and $\mathcal{D}_y = [0, x_{\text{max}}] \times [0, l_y]$ (represented in green). The extrapolation is performed in two steps: first, we perform a CI decomposition of f inside \mathcal{D}_c with χ pivots. We obtain an approximation of the form (3) for $x, y \in \mathcal{D}_c$ where the pivots are in \mathcal{D}_c . Second, we use Eq. (3) to extrapolate the function f to the whole domain \mathcal{D} . Indeed, the calculation of $f_\chi^{\text{CI}}(x, y)$ for any $x, y \in \mathcal{D}$ (e.g. the purple star point in Fig. 2) uses only the values of f on the L -shape domain \mathcal{D}_{sub} .

A central question in such an algorithm is the potential amplification of errors in the extrapolation. In particular,

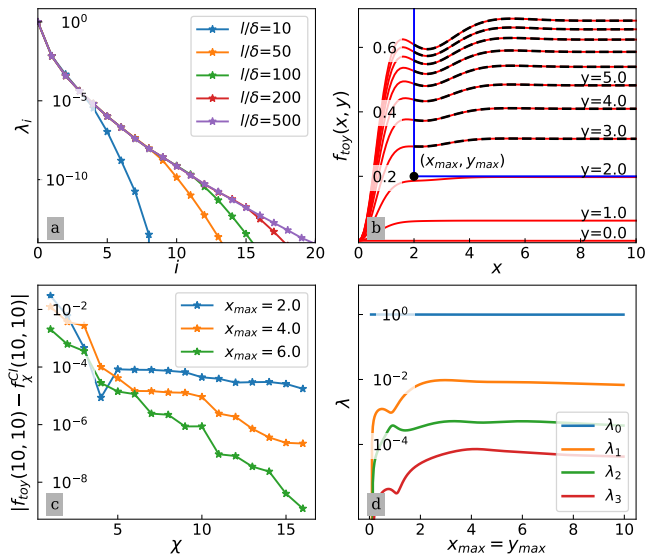


Figure 3. Benchmark of the cross-extrapolation algorithm on a L -shaped domain with f_{toy} . (a) Singular values λ_i (normalized by $\sum \lambda_i$) of f_{toy} vs i for various numbers of grid points l/δ per dimension. In other panels, one sets $l/\delta = 100$ (b) Comparison of f_{toy} with its reconstructed value with cross-extrapolation for $x > x_{\text{max}}, y > y_{\text{max}}$, for $x_{\text{max}} = y_{\text{max}} = 2$, using $\chi = 5$ pivots; the black dashed curve is the extrapolation, the red curve is f_{toy} . (c) Error of the extrapolation at $x = y = 10$ vs the rank χ for three values of x_{max} . (d) Four largest singular values of f_{toy} inside the subdomain $\mathcal{D}_c = [0, x_{\text{max}}] \times [0, y_{\text{max}}]$ versus x_{max} for $x_{\text{max}} = y_{\text{max}}$.

we expect that if the subdomain is too small, the pivot matrix will become too singular (i.e. with very small singular value) to allow an accurate reconstruction. Indeed, even in the case where the extrapolation is mathematically exact (the function is exactly of rank χ), the extrapolation is expected to fail in practice if the size of the subdomain becomes too small, if only because of the rounding error in e.g. double precision calculations will ultimately get amplified by the fact that the pivot matrix will get highly ill conditioned. In real case calculations the function will be known with finite precision. In order to illustrate this point, we benchmark the cross-extrapolation algorithm on a simple (toy) function, constructed to have a shape similar to the real case physical quantity that we will study later,

$$f_{\text{toy}}(x, y) = \left(\frac{x}{x+1}\right)^4 (1 + e^{-y^2}) [1 + y \cos(y)e^{-y \frac{x}{x+1}}] \quad (5)$$

where $\mathcal{D} = [0, l_x] \times [0, l_y]$ with $l_x = l_y = l = 10$. The results are presented on Fig. 3. First we check that the function f_{toy} is actually of low ϵ -rank, by computing the SVD of the matrix obtained by discretizing it on a uniform grid with spacing δ (l/δ grid points per dimension). The (sorted) singular values λ_i are shown on Fig. 3a, versus index i , for different grid discretization. We observe that λ_i decreases very quickly with i (i.e. the function is of

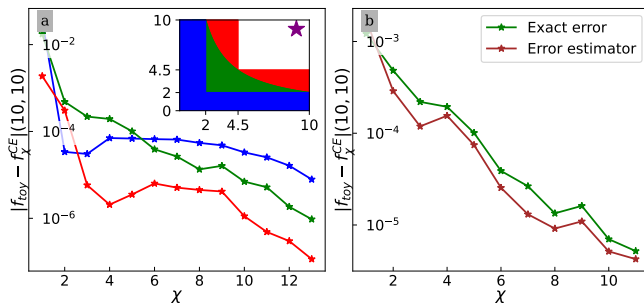


Figure 4. (a) Cross-extrapolation error at $(x = 10, y = 10)$ for three domains: an hyperbolic domain (green \cup blue) and two L -shaped domains (blue, red \cup green \cup blue). The color of the curve correspond to the color of the domain. b) Error estimator ϵ_{χ} (red) and exact error (green) at $(x = 10, y = 10)$ as a function of χ for the green domain using $N_{\chi} = 3$.

low rank to a very good approximation), and that they converge with the grid discretization $\delta \rightarrow 0$.

Second, we compare f_{toy} to the reconstructed function f_{χ}^{CI} with the cross-extrapolation from the L -shaped domain (with $x_{max} = y_{max} = 2$) to the whole domain. Fig. 3b shows a perfect match between the extrapolation (black dashed line) and the actual function (thin red) despite the fact that the extrapolation is non-trivial.

The corresponding extrapolation error $|f_{toy} - f_{\chi}^{CI}|$ [for $(x, y) = (10, 10)$] versus the rank χ is shown in Fig. 3c. We observe a quick convergence of the error when χ is increased. The convergence is faster when we use more information, i.e. for larger x_{max} . A simple way to understand the role of the size of the subdomain (here given by $x_{max} = y_{max}$) is to compute the SVD of the function (on a thin grid) on the \mathcal{D}_c subdomain, as a function of x_{max} . This is presented on Fig. 3d. For small x_{max} , the singular values are very small, increase with x_{max} and then saturate. If the subdomain is too small, the singular values of the function in it becomes very small, and the cross-extrapolation is expected to fail due to error amplification. Qualitatively, Fig. 3d provides a good *a priori* indication of how well cross-extrapolation will perform: in a favourable case, one can have access to values of x_{max} large enough so that the singular values of the pivot matrix have already developed into a plateau; at the same time, the faster the singular value λ_i decays with i , the better. See Fig. 12 in Appendix A for a step by step illustration of the cross-extrapolation from a L -shaped domain.

2. General subdomain and error estimation

In practice, the subdomain \mathcal{D}_{sub} where the function can be calculated can be more complex than a simple L -shape and we now extend the cross extrapolation algorithm to handle a more general case. We shall illustrate the general algorithm in the case where \mathcal{D}_{sub} is the area underneath an hyperbole $xy < c$, where c is some constant, which we

will refer to as *hyperbolic subdomain*, see the schematic in Fig. 2b.

Simply applying the L shape algorithm here would be inefficient as it would not use all the available information on the function. Our generalized algorithm works as follows (see Fig. 2b for an illustration). We start from $\mathcal{D}_x = [0, z] \times [0, c/z]$ and use the L -shape algorithm to extrapolate the function to obtain it just one line up (\mathcal{D}_x becomes $\mathcal{D}_x = [0, z] \times [0, c/z + \delta]$). One continues the extrapolation up line by line, reusing the extrapolated results of previous lines, until one has reached $y = z$. Crucially, the extrapolated points (in deep blue in Fig. 2b) are reused only for the \mathcal{D}_x domain of subsequent extrapolations, but never for the \mathcal{D}_c domain, as we observe that it would lead to instabilities. With this approach, the pivot region \mathcal{D}_c is still rectangular, but evolves along the computation to make use of the entire available information on the function. We denote by f_{χ}^{CE} the resulting Cross Extrapolation at rank χ . Figure 13 in Appendix A provides a step by step illustration of the algorithm.

In Fig. 4, we present some benchmark using an hyperbolic domain for reconstructing f_{toy} . On the left panel, we show the error between the f_{toy} and f_{χ}^{CE} , for two L -shape subdomains (blue and red) and the hyperbolic subdomain (green). As expected, we observe that the convergence is faster for larger subdomain at large χ : the errors are ordered in the opposite way compared to the inclusion relation of the corresponding domains (blue \subset green \cup blue \subset red \cup green \cup blue). In our experiments, we have not observed any decrease of accuracy of the generalized algorithm with respect to the L -shape algorithm (no amplification of error due to the reusing of extrapolated values for subsequent extrapolations). However, it is very important that at any stage the \mathcal{D}_c domain satisfies $xy < c$; indeed, the algorithm becomes unstable when one uses pivots whose values have already been extrapolated (i.e. from the deep blue region of Fig.2b).

Let us now discuss an estimator of the extrapolation error. In the simple toy model case where the function is known exactly in \mathcal{D}_{sub} , the error is controlled by the rank χ . We use N_{χ} consecutive values of χ to estimate it. In theory, $N_{\chi} = 2$ is sufficient but it sometimes leads to fluctuations in the error due to accidental coincidence of the two estimates. In addition, $N_{\chi} = 2$ supposes that the error is dominated by the next singular value, i.e. that they decrease rapidly. Hence, in practice we often use $N_{\chi} = 3$ or 4. Anticipating on real case applications, a second source of error comes from the function being only known approximately inside \mathcal{D}_{sub} with an error η . Hence, we further generate N_{η} extrapolations $f_{\chi, j}^{CE}(x, y)$ corresponding to N_{η} different estimations of the function inside \mathcal{D}_{sub} ($N_{\eta} = 1$ for the toy function). Our estimate of the error ϵ_{χ} of the extrapolation at point (x, y) reads,

$$\epsilon_{\chi} = \max_{\substack{i, i' \in \{0 \dots N_{\chi} - 1\} \\ j, j' \in \{1 \dots N_{\eta}\}}} |f_{\chi+i, j}^{CE}(x, y) - f_{\chi+i', j'}^{CE}(x, y)| \quad (6)$$

Fig. 4b shows ϵ_{χ} versus χ for the toy function together with the actual the exact error (deviation from the cross-

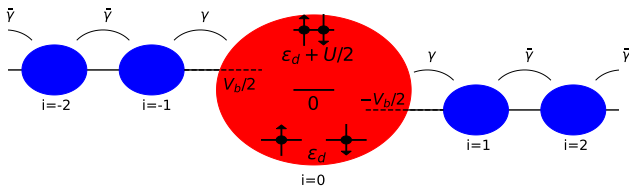


Figure 5. The Single Impurity Anderson Model : a single-level quantum dot on site $i = 0$ with on-site energy ϵ_d is subject to a finite Coulomb interaction U and is hybridized with a tunnel coupling γ with two semi-infinite leads ($i > 0$ and $i < 0$) that are biased with voltage $\pm V_b/2$. The hopping $\bar{\gamma}$ on the electrodes is such that $\gamma \ll \bar{\gamma}$

extrapolation to the original function) which is known in the toy example. We find that the estimate is close to the exact error, and we will use this error estimator in the following.

The cross-extrapolation algorithm for two variables is *a priori* general. Its success is linked to a property - low rankness - that we observe in the model below and conjecture to be present in a large variety of similar situations. Our numerical experiments suggest that the method is robust: if we try it on a function which is *not* low rank, we immediately observe a large increase of the error estimate. Furthermore, the low rankness of the function can already be assessed inside \mathcal{D}_{sub} using the analysis done in Fig. 4d. Note however that, from a strictly mathematical point of view, the low-rank property of the function is not sufficient for the extrapolation to be controlled. A simple failure example would be $f(x, y) = \theta(x - 1)\theta(y - 1)$ which can not be extrapolated from the sub-domain $\mathcal{D}_{\text{sub}} = \{x < 1\} \cup \{y < 1\}$.

III. APPLICATION TO THE EXTRAPOLATION OF TIME-DEPENDANT SERIES

Let us now turn to the reconstruction of physical quantities from their perturbative series at finite time t . We study a well established model, the single quantum impurity Anderson model (SIAM) for a quantum dot. The SIAM is directly relevant experimentally, contains non-trivial Kondo physics, is well understood at equilibrium (with exact benchmarks) while still under active study out-of-equilibrium [2, 40–42]. The SIAM corresponds to a single interacting level (site 0) weakly connected to two one dimensional leads ($i > 0$ and $i < 0$, see the schematic on Fig. 7). Its Hamiltonian reads,

$$\hat{H} = \epsilon_d(\hat{n}_\uparrow + \hat{n}_\downarrow) + U\theta(t)(\hat{n}_\uparrow - \alpha)(\hat{n}_\downarrow - \alpha) + \sum_{\substack{i \in \mathbb{Z} \\ \sigma = \uparrow, \downarrow}} \gamma_i c_{i,\sigma}^\dagger c_{i+1,\sigma} + \text{h.c.} \quad (7)$$

where $c_{i,\sigma}^\dagger$ ($c_{i,\sigma}$) creates (destroys) an electron on site i with spin σ , ϵ_d is the on-site energy, $\hat{n}_\sigma \equiv \hat{c}_{0,\sigma}^\dagger \hat{c}_{0,\sigma}$ is the

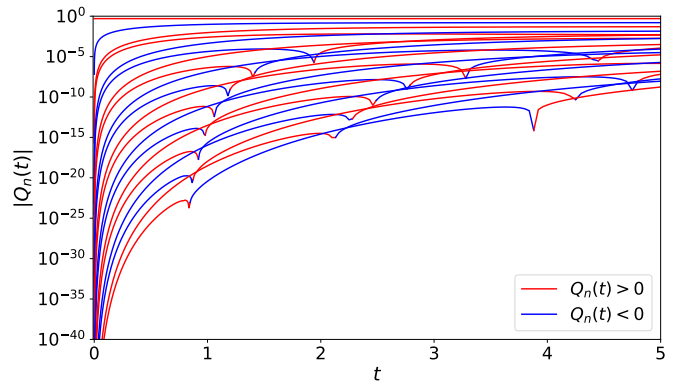


Figure 6. Coefficients $Q_n(t)$ versus t calculated with the TTD method for $\alpha = \epsilon_d = 0$. From top to bottom the order n increases from $n = 0$ to $n = 19$. The color corresponds to positive (red) and negative (blue) values of the coefficient, the kinks to change of sign (the kinks get more pronounced upon adding more values of t on the grid). The relative error on the coefficients is of the order of 10^{-8} for $n = 6$ and 10^{-5} for $n = 19$, it is much smaller than the width of the lines. Note the very large dispersion in magnitude of the coefficients. The coefficients are shown up to $t = 5$ but can be computed for arbitrary large t at no additional cost. Note that four different runs were needed in order to have access to both large and small times with sufficient accuracy due to the smallness of the coefficients at small time and large order (starting from $t = 0$ with final times $t = 0.01$, $t = 0.1$, $t = 1$ and $t = 5$).

density of electron in the impurity and U the strength of interaction between electrons which is switched on at $t = 0$. $\gamma_i = \bar{\gamma}$ except for the coupling to the dot $\gamma_0 = \gamma_{-1} = \gamma$. The calculations are performed in the weak coupling limit $\gamma \ll \bar{\gamma}$ where the energy dependence of the leads can be ignored (flat band approximation). The system can be put out-of-equilibrium in two ways: using a symmetric voltage difference $\pm V_b/2$ across the leads and using a quench of the interaction. All times are written in unit of Γ^{-1} with $\Gamma = 2\frac{\gamma^2}{\bar{\gamma}}$. The *shift parameter* α does not affect the overall Hamiltonian as it can be absorbed in the on-site energy: $\hat{H}(\epsilon_d, \alpha) = \hat{H}(\epsilon_d - \alpha U, 0)$ up to a constant energy shift. However, it allows one to perform several different expansions in power of U to reach the same final result (keeping $\epsilon_d - \alpha U = \text{const}$), but with different radius of convergence at infinite time t [5].

A. Charge of the quantum dot in equilibrium. Benchmark

Let us first consider the charge on the quantum dot, at zero temperature $T = 0$, in equilibrium (no voltage bias). This quantity is a good benchmark for the technique, because we have Bethe Ansatz exact results for it at $t = \infty$ (see Fig. 1) [43] and it is an easy case of the conformal mapping resummation technique [1, 5]. In addition to

this benchmark, we will also obtain the transient out-of-equilibrium regime at finite time t after the quench, a non-trivial calculation. The charge is given by the expansion,

$$Q(U, t) = \langle \hat{n}_\uparrow + \hat{n}_\downarrow \rangle \approx \sum_{n=0}^N Q_n(t) U^n \quad (8)$$

where only a finite number N of coefficients $Q_n(t)$ are known. The extrapolation problem consists in extrapolating to the $N \rightarrow \infty$ limit. The calculation of the coefficient $Q_n(t)$ involves n -dimensional integrals of a function consisting an exponentially large number of terms [5, 20, 21]. We use the tensor train diagrammatic (TTD) method within the real-time Keldysh formalism to compute this expansion [20]. Indeed, tensor network methods enable the computation of perturbative expansions of observables of this model to unrivalled orders ($N \leq 30$) and accuracies [20, 40]. Also, TTD provides the full time dependence in a single calculation [20]. The coefficients $Q_n(t)$ calculated with TTD are shown in Fig. 6. The frequent changes of sign indicates the presence of a sign problem that would make such a calculation at that precision impossible with Monte-Carlo. Also note the scale of the y -axis while the typical error bar is smaller than the width of the line.

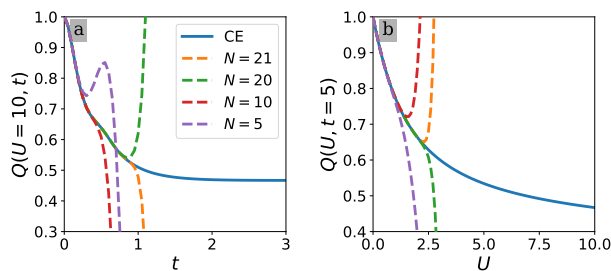


Figure 7. Charge $Q(U = 10, t)$ vs t (panel a), and $Q(U, t = 5)$ vs U (panel b) calculated with bare summation (dashed lines, colors correspond to different values of N) and the extrapolation using $N = 21$ (plain blue line).

At infinite time, the perturbative series has a finite radius of convergence R ,

$$\lim_{t \rightarrow \infty} Q_n(t) \sim \frac{1}{R^n} \quad (9)$$

and previous works have focused on the resummation of the series in this limit [1]. However, at *any finite time*, the series has an infinite radius of convergence [1], as the coefficients are bounded as

$$Q_n(t) = O\left(\frac{t^n}{n!}\right). \quad (10)$$

For $Ut < c$, the finite N approximation is therefore converged for $N > c/a$ up to an exponentially small error of order $(c/aN)^N$, where a is a numerical coefficient of order unity. These properties of the series are illustrated on Fig. 7, which shows, for the charge $Q(U, t)$, the exact

value (computed below), and the bare perturbative series summation for a finite number of order N . At fixed large interaction U , the series is actually convergent, but the longer the time, the more orders are needed to achieve convergence, see Fig. 7a. At infinite time, the series has finite radius of convergence, which manifests itself by a divergence of the finite N sum at finite large time t , see Fig. 7b.

Our strategy is to compute $Q(U, t)$ in the hyperbolic domain \mathcal{D}_{sub} defined by

$$Ut < c \quad (11)$$

and use the cross-extrapolation algorithm to obtain Q at larger times and interactions. Since the computation of the coefficients in the Keldysh formalism scales as 2^n , we have access to a limited number $N \leq 30$ of them at best ($N \approx 30$ takes a few tens of hours and hundred computing cores, we use $N = 20 - 25$ in practice for reasonable computational times) which sets the maximum value of c that is actually reachable. The results of the extrapolation are shown in Fig. 8. In order to check the stability of the algorithm, we vary the parameter c . If c is too small, as discussed earlier, \mathcal{D}_{sub} is too small, leading to an almost singular pivot matrix and unstable extrapolation. In practice, we obtain different results for different values of the rank χ . If c is too large, the number of coefficients N will be too small to converge the series in \mathcal{D}_{sub} (hence varying N yields different results). The results are shown in Fig. 8a for various values of χ (different colors) and two different values of N (full versus dashed lines). As c increases, we observe a convergence of the extrapolated result. Using large value of χ requires large values of c (here the $\chi = 4$ curve is barely converged at $c = 8$ while $\chi = 2$ converges already at $c > 5$) so the extrapolation will be most efficient for functions where small values $\chi = 1$ or 2 already provide a good extrapolation. For $c > 8$, we do not have enough coefficients for convergence and the results become N dependent.

In practice, we look for the optimal value of $c = c_{\text{opt}}$ for which the estimated error $\epsilon_X(c)$ is minimal, see Fig. 8b ($c_{\text{opt}} \approx 8$ in this example). Here we have used $N_\chi = 3$ and $N_\eta = 2$ (two values $N = 20$ and 21) for the calculation of $\epsilon_X(c)$. Notice that our error estimate (blue) is conservative versus the true error (orange) that we can obtain for this benchmark using Bethe Ansatz. The final extrapolation versus time t is presented for different U in Fig. 8c (see also Fig. 1a for a 2D colorplot and Fig. 1b for the large time limit versus U , in quantitative agreement with the Bethe Ansatz benchmark). While the asymptotic result was known already from previous work, the full curve Fig. 8c is a non-trivial out-of-equilibrium calculation of an interaction quench. Notice the kink that seems to develop around $t \approx 0.8$ at large U (whose physical interpretation we leave to future work).

An important property of the cross-extrapolation approach (as opposed to conformal transform as we shall discuss below) is that it can be systematically improved by computing more orders. This is checked in Fig. 9 where

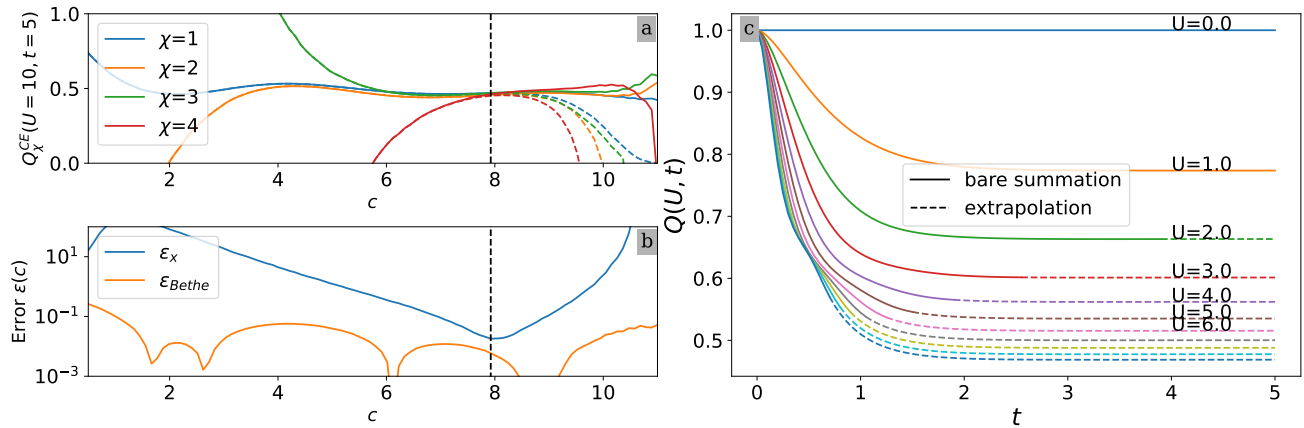


Figure 8. (a) $Q_x^{CE}(U = 10, t = 5)$ versus c , for $\chi = 1, 2, 3, 4$ with $\alpha = \epsilon_d = V_b = 0$ and $N = 21$ (resp. $N = 20$) coefficients of the perturbative series in plain (resp. dashed) line. (b) Error estimator $\epsilon_x(c)$ (in blue) versus c for the quantity plotted in panel (a) and exact error ϵ_{Bethe} (orange). The exact error has been computed using the exact Bethe Ansatz series using the Euler conformal transformation method [22]. The black dashed line marks the minimum of the error c_{opt} . (c) $Q(U, t)$ obtained by the bare series, while dashed line sections are obtained by cross-extrapolation. For all panels, we use a 100×100 grid and $c_{opt} = 7.9$.

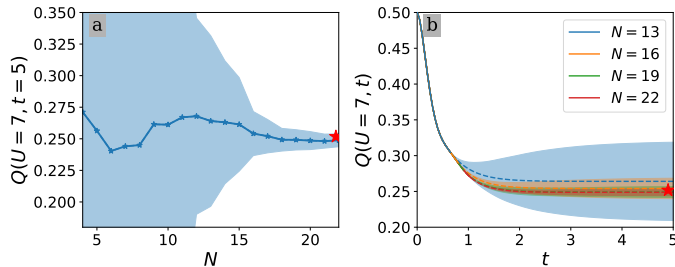


Figure 9. (a) Charge Q^{CE} vs N , for $\alpha = \epsilon_d = V_b = 0$ at $U = 7$ and $t = 5$. Error bars from CE are given by the shaded area. The red star is obtained using conformal maps. (b) Charge Q^{CE} vs t , for $U = 7$ and different values of N . Plain (resp. dotted) lines correspond to bare summation (resp. extrapolation).

we study the influence of N (the number of orders) by plotting the charge obtained by cross-extrapolation Q^{CE} for different values of N and time t . We observe that the error bar quickly decreases with N for a given time, see Fig. 9a. As a function of t , we see that the error is small at short time, larger at long time, but also significantly decreases when N increases, see Fig. 9b.

B. Current through the quantum dot

We now turn to the calculation of the current flowing through the quantum dot to the right electrode. The interaction quench takes the system from a non-equilibrium non-interacting steady state to a non-equilibrium interacting steady state. We want to compute both the steady state in the presence of voltage at long time, and its transient regime after the interaction quench. Since

we have no benchmark here, we perform several calculations varying the shift parameter α , using different pairs (ϵ_d, α) such that $\epsilon_d - 7\alpha = 2$, which must produce the same result at $U = 7$. The calculation of the current $I(V_b = 2, \epsilon_d = 2, \alpha = 0, U = 7)$ is presented in Fig. 10a. All calculations of I indeed coincide (the red star) within their respective error bars. Some extrapolations have relatively large error bars (the worst is $\alpha = 0$ which becomes rather inaccurate for $U > 4$), others are more precise (the best is $\alpha = 0.5$) and could be pushed to much larger values of U (above $U = 10$ in this case).

Fig. 10b show the same data versus time for the different quenches and $U = 7$. All the different quenches converge to the same value, as they should, within the calculated error bars (see Fig. 10c for a zoom of the asymptotic regime, the error bar for $\alpha = 0.5$ is too small to be visible). The results of Fig. 10 show that we have now access to out-of-equilibrium observables, away from the perturbative regime, and for a wide range of parameters (before [20], only a narrow region in ϵ_d could be computed). We defer to a subsequent publication a full study of the physics made available by this combination of TTD and the cross-extrapolation.

Let us now compare the cross-extrapolation with the technique used in previous works, conformal transformation [1]. Conformal transformation uses the series at $t = \infty$,

$$Q(U, t = \infty) = \sum_{n=0}^{\infty} Q_n(t = \infty) U^n \quad (12)$$

which we have also calculated for the same parameters (in practice, the calculations are performed at a finite time that satisfies $t \gg n$, the computation time does not depend on this choice). The series has a finite radius of convergence R , hence the summation in Eq.(12) diverges

for $U > R$ as one increases the number of coefficients N kept in the calculation. The strategy of the conformal transform is to locate the poles in the complex U plane ($\text{Re}(U), \text{Im}(U)$) that are responsible for the finite radius of convergence, then design a conformal transformation that send these poles away while bringing the value of U for which we want to calculate the observable (U_{phys}) closer to the origin [1]. In our experience, the conformal transform yields spectacular results when the poles are situated on the left of the origin $\text{Re}(U) < 0$ when one wants to calculate the observable for $\text{Re}(U) > 0$: in that case, there is a clear separation between the poles and U_{phys} and $N = 10 - 12$ coefficients with 1% accuracy can be sufficient to calculate the observable up to large U , even $U = \infty$ [5]. However, when the poles get closer to the points of interest (the poles lie on the right of the origin $\text{Re}(U) > 0$), the conformal transform fails (but not silently). In such case, computing more orders (up to $N \approx 25$ as in the present work) or even radically improving the accuracy of the calculation (up to 10^{-8} relative precision in the present work compared to $10^{-2} - 10^{-3}$ with Monte-Carlo sampling) does not really change the outcome.

Remarkably, the cross-extrapolation can succeed when the conformal technique fail. The computation of the current I illustrates this. Fig. 10d shows the positions of the poles of $Q(U, t = \infty)$ in the ($\text{Re}(U), \text{Im}(U)$) plane, and the different radius of convergences for various α . The poles lie in the $\text{Re}(U) > 0$ part of the plane. As a result, we cannot perform the resummation using conformal transformations in this case, while the cross-extrapolation works perfectly. Furthermore, cross-extrapolation systematically takes advantage of more orders (increase the time up to which the observable can be computed) and more accuracy (increases the range where the observable can be extrapolated).

IV. CONCLUSION

We have shown that some physical quantities on the non-equilibrium Anderson model, when considered as a function of U and t are of low-rank. Furthermore, perturbative techniques give us access the short time regime (for a large range of U) and the small interaction regime (for any time t). Due to the low-rank property, we

have shown that the knowledge of the function in these two regimes is sufficient to extrapolate it reliably at long time and strong coupling.

In order to perform this calculation, we have presented a general-purpose *cross-extrapolation* algorithm to extrapolate a low rank function of two variables from a small domain to a larger one, i.e. perform *two-variables* extrapolations. In our experience, this algorithm is rank-revealing i.e. it does not fail silently: when the function is not low rank or the computed domain is too small, the error bar simply increases until the extrapolation is no longer useful. We expect this algorithm to be of general use, beyond the special case discussed in this paper, in condensed matter physics or beyond. It could also potentially be extended to more than two variables using the tensor cross interpolation [20].

We have shown that the cross-extrapolation is able to reconstruct some physical quantities at strong coupling in a case where the previously established approach based on conformal maps [5] fails. Furthermore, in contrast with the conformal maps, it can be systematically improved by calculating more coefficients (although the computational cost scales as 2^N) and it can be largely automatized, which is crucial for potential future application to self-consistent methods such as non-equilibrium dynamical mean field theory [44].

Finally, we conjecture that the crucial low-rank properties of physical quantities in the (U, t) plane is a general properties of similar models. In particular, in the context of equilibrium diagrammatic QMC, it will be very interesting to examine the rank of physical properties in terms of interaction U and inverse temperature β , as we expect β to play a similar role of infra-red regulator as the time t in the out-of-equilibrium context. In practice, we could even use two different but complementary techniques, one to compute the small U regime and another one to compute the small β regime.

V. ACKNOWLEDGEMENTS

The Flatiron Institute is a division of the Simons Foundation. XW acknowledges funding from the Plan France 2030 ANR-22-PETQ-0007 ‘‘EPIQ’’, from the French ANR DADDI and from the AI program of the French MESRI.

-
- [1] C. Bertrand, S. Florens, O. Parcollet, and X. Waintal, Reconstructing nonequilibrium regimes of quantum many-body systems from the analytical structure of perturbative expansions, *Phys. Rev. X* **9**, 041008 (2019), [arXiv:1903.11646](#).
 - [2] C. Bertrand, D. Bauernfeind, P. T. Dumitrescu, M. Macek, X. Waintal, and O. Parcollet, Quantum quasi monte carlo algorithm for out-of-equilibrium green functions at long times, *Physical Review B* **103**, 10.1103/physrevb.103.155104 (2021).
 - [3] A. F. Kemper, C. Yang, and E. Gull, On the positive definiteness of response functions in the time domain (2023), [arXiv:2309.02566 \[quant-ph\]](#).
 - [4] A. J. Guttmann, Asymptotic analysis of power-series expansions, in *Phase Transitions and Critical Phenomena*, Vol. 13, edited by T. editor (C. Domb and J. Lebowitz, Academic, New York, 1989) pp. 201–213.
 - [5] R. E. V. Profumo, C. Groth, L. Messio, O. Parcollet, and X. Waintal, Quantum monte carlo for correlated out-of-equilibrium nanoelectronic devices, *Phys. Rev. B* **91**,

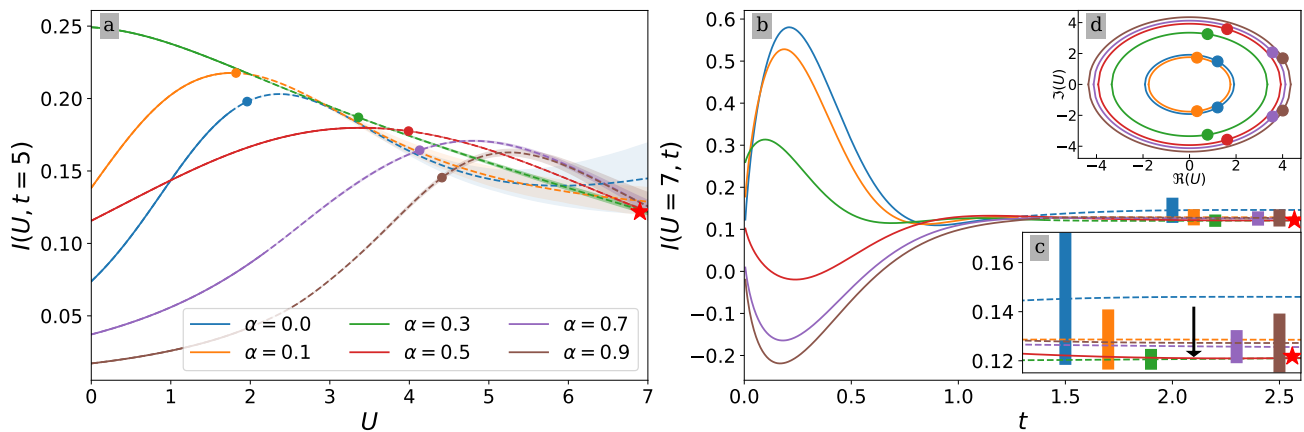


Figure 10. (a) Current vs U for various values of α and ϵ_d so that the on-site energy at $U = 7$ verifies $\epsilon_d - 7\alpha = 2$ with bias voltage $V_b = 2$ and using $N = 21$ coefficients. The different curves should and do converge to a single point at $U = 7$ (the red star). Full lines correspond to the simple plain summation of the N coefficient; they turn into dashed lines when the extrapolation starts. The circles indicate the position of the radius of convergence of the corresponding series at infinite time (above this point the bare series diverges). The shaded areas indicate the error bars. (b) Same data as a function of time t for $U = 7$ and various α values. The color rectangles show the error bars for the curve of the corresponding color. The error for the red curve $\alpha = 0.5$ is small and not visible at this scale (c) zoom of (b) in the extrapolation region. Note that $\alpha = 0.5$ is the most precise prediction (the error bar is of the order of the line width at the position indicated by the arrow) and $\alpha = 0$ the worst. (d) Position of the poles of the asymptotic series in the complex plane ($\text{Re}(U)$, $\text{Im}(U)$) for the same series in the large t limit.

- 245154 (2015).
- [6] R. Rossi, N. Prokof'ev, B. Svistunov, K. V. Houcke, and F. Werner, Polynomial complexity despite the fermionic sign, *Europhysics Letters* **118**, 10004 (2017).
- [7] R. Rossi, T. Ohgoe, K. Van Houcke, and F. Werner, Resummation of diagrammatic series with zero convergence radius for strongly correlated fermions, *Phys. Rev. Lett.* **121**, 130405 (2018).
- [8] C. Brezinski, Extrapolation algorithms and padé approximations: a historical survey, *Applied Numerical Mathematics* **20**, 299 (1996).
- [9] G. Baker and P. Graves-Morris, *Padé Approximants*, Encyclopedia of Mathematics and its Applications, Vol. 59 (Cambridge University Press, 1996).
- [10] O. Costin and G. V. Dunne, Resurgent extrapolation: rebuilding a function from asymptotic data. painlevé i, *Journal of Physics A: Mathematical and Theoretical* **52**, 445205 (2019).
- [11] K. V. Houcke, F. Werner, T. Ohgoe, N. V. Prokof'ev, and B. V. Svistunov, Diagrammatic monte carlo algorithm for the resonant fermi gas, *Physical Review B* **99**, 10.1103/physrevb.99.035140 (2019).
- [12] *Séries divergentes et procédés de resommation*, *Journées X-UPS* (Ecole Polytechnique, Palaiseau, France, 1991).
- [13] S. Gluzman, V. I. Yukalov, and D. Sornette, Self-similar factor approximants, *Phys. Rev. E* **67**, 026109 (2003).
- [14] V. I. Yukalov, E. P. Yukalova, and S. Gluzman, Extrapolation and interpolation of asymptotic series by self-similar approximants, *Journal of Mathematical Chemistry* **47**, 10.1007/s10910-009-9618-1 (2010), 1004.1041.
- [15] N. V. Prokof'ev and B. V. Svistunov, Bold diagrammatic monte carlo: A generic sign-problem tolerant technique for polaron models and possibly interacting many-body problems, *Phys. Rev. B* **77**, 125101 (2008).
- [16] E. Lindelöf, *Le Calcul des Résidus et ses Applications à la Théorie des Fonctions* (Gauthier-Villars, Paris, 1905).
- [17] N. V. Prokof'ev and B. V. Svistunov, Polaron problem by diagrammatic quantum monte carlo, *Phys. Rev. Lett.* **81**, 2514 (1998).
- [18] K. Van Houcke, E. Kozik, N. Prokof'ev, and B. Svistunov, Diagrammatic monte carlo, *Physics Procedia* **6**, 95 (2010), computer Simulations Studies in Condensed Matter Physics XXI.
- [19] K. V. Houcke, F. Werner, E. Kozik, N. Prokof'ev, B. Svistunov, M. J. H. Ku, A. T. Sommer, L. W. Cheuk, A. Schirrotzek, and M. W. Zwierlein, Feynman diagrams versus fermi-gas feynman emulator, *Nature Physics* **8**, 366 (2012).
- [20] Y. Núñez Fernández, M. Jeannin, P. T. Dumitrescu, T. Kloss, J. Kaye, O. Parcollet, and X. Waintal, Learning feynman diagrams with tensor trains, *Phys. Rev. X* **12**, 041018 (2022).
- [21] C. Bertrand, O. Parcollet, A. Maillard, and X. Waintal, Quantum Monte Carlo algorithm for out-of-equilibrium Green's functions at long times, *Phys. Rev. B* **100**, 125129 (2019), arXiv:1903.11636.
- [22] M. Maček, P. T. Dumitrescu, C. Bertrand, B. Triggs, O. Parcollet, and X. Waintal, Quantum quasi-monte carlo technique for many-body perturbative expansions, *Physical Review Letters* **125**, 047702 (2020).
- [23] F. Simkovic, R. Rossi, and M. Ferrero, Two-dimensional hubbard model at finite temperature: Weak, strong, and long correlation regimes, *Phys. Rev. Res.* **4**, 043201 (2022).
- [24] F. Simkovic, R. Rossi, A. Georges, and M. Ferrero, Origin and fate of the pseudogap in the doped hubbard model (2022), arXiv:2209.09237 [cond-mat.str-el].
- [25] L. Lin and S. R. White, A novel method of function extrapolation inspired by techniques in low-entangled many-body physics (2023), arXiv:2308.09001 [quant-ph].
- [26] M. K. Ritter, Y. N. Fernández, M. Wallerberger, J. von Delft, H. Shinaoka, and X. Waintal, Quantics tensor cross interpolation for high-resolution, parsimonious represen-

- tations of multivariate functions in physics and beyond (2023), [arXiv:2303.11819 \[physics.comp-ph\]](#).
- [27] F. R. Gantmacher, *The Theory of Matrices* (Chelsea Publishing Company, 1960).
- [28] S. Goreinov, E. Tyrtyshnikov, and N. Zamarashkin, A theory of pseudoskeleton approximations, *Linear Algebra and its Applications* **261**, 1 (1997).
- [29] N. K. Kumar and J. Schneider, Literature survey on low rank approximation of matrices, *Linear and Multilinear Algebra* **65**, 2212 (2017).
- [30] K. Hamm and L. Huang, Perspectives on cur decompositions, *Applied and Computational Harmonic Analysis* **48**, 1088 (2020).
- [31] M. W. Mahoney and P. Drineas, Cur matrix decompositions for improved data analysis, *Proceedings of the National Academy of Sciences* **106**, 697 (2009).
- [32] M. Xu, R. Jin, and Z.-H. Zhou, Cur algorithm for partially observed matrices (2014), [arXiv:1411.0860 \[cs.LG\]](#).
- [33] S. A. Goreinov, N. L. Zamarashkin, and E. E. Tyrtyshnikov, Pseudo-skeleton approximations by matrices of maximal volume, *Mathematical Notes* **62**, 515 (1997).
- [34] S. Goreinov and E. Tyrtyshnikov, The maximal-volume concept in approximation by low-rank matrices, *Contemporary Mathematics* **208** (2001).
- [35] S. A. Goreinov, I. V. Oseledets, D. V. Savostyanov, E. E. Tyrtyshnikov, and N. L. Zamarashkin, How to find a good submatrix, in *Matrix Methods: Theory, Algorithms and Applications* (World Scientific, 2010) pp. 247–256.
- [36] S. Dolgov and D. Savostyanov, Parallel cross interpolation for high-precision calculation of high-dimensional integrals, *Computer Physics Communications* **246**, 106869 (2020).
- [37] M. Bebendorf, Approximation of boundary element matrices, *Numerische Mathematik* **86**, 565 (2000).
- [38] M. Bebendorf, Adaptive cross approximation of multivariate functions, *Constructive Approximation* **34**, 149 (2011).
- [39] J. Schneider, Error estimates for two-dimensional cross approximation, *Journal of Approximation Theory* **162**, 1685 (2010).
- [40] A. Erpenbeck, W. T. Lin, T. Blommel, L. Zhang, S. Isakov, L. Bernheimer, Y. Núñez-Fernández, G. Cohen, O. Parcollet, X. Waintal, and E. Gull, A tensor train continuous time solver for quantum impurity models (2023), [arXiv:2303.11199 \[cond-mat.str-el\]](#).
- [41] M. M. Wauters, C.-M. Chung, L. Maffi, and M. Burrello, Simulations of the dynamics of quantum impurity problems with matrix product states (2023), [arXiv:2304.13756 \[cond-mat.str-el\]](#).
- [42] M. Vanhovecke and M. Schirò, Diagrammatic monte carlo for dissipative quantum impurity models (2023), [arXiv:2311.17839 \[cond-mat.str-el\]](#).
- [43] P. B. Wiegmann and A. M. Tsvelick, Exact solution of the anderson model: I, *Journal of Physics C: Solid State Physics* **16**, 2281 (1983).
- [44] A. Georges, G. Kotliar, W. Krauth, and M. J. Rozenberg, Dynamical mean-field theory of strongly correlated fermion systems and the limit of infinite dimensions, *Rev. Mod. Phys.* **68**, 13 (1996).

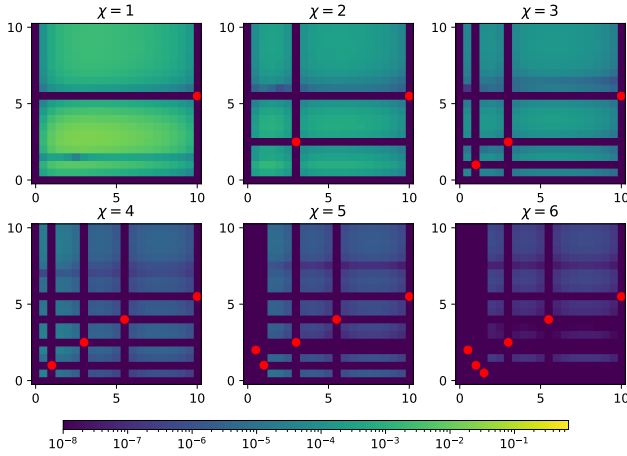


Figure 11. Error versus x and y at different stages of the Cross-Interpolation. The illustration is done on the function f_{toy} defined in Eq. (5) on a uniform 20×20 grid for $(x, y) \in [0, 10]^2$. The red dots indicate the pivots.

Appendix A: Illustration of cross-interpolation and cross-extrapolation

In this appendix, we show a step by step illustrations of the different algorithms in the context of our toy function Eq.(5). The figures show the error of the approximation at different stage of the calculation upon increasing the rank χ . The red circles show the positions of the pivots and the function has been discretized on a coarse 20×20 grid (for visibility).

- Fig. 11 shows the cross-interpolation algorithm (the function is known everywhere, $\mathcal{D}_{\text{sub}} = \mathcal{D}$). The pivots are added one by one by selecting the position where the error is maximum. This strategy is known as the Adaptive Cross Approximation (ACA) [37] and is near-optimal.
- Fig. 12 shows the L -shape cross-extrapolation algorithm for the same function. Here the pivots can only be inside the red square and we seek an extrapolation inside the white square. We observe that the algorithm converges, although not as fast as cross-interpolation.
- Fig. 13 shows the general-shape cross-extrapolation algorithm for the same function using the hyperbolic domain $xy < 25$ and $\chi = 3$. The different panels (from left to right then top to bottom) show the line by line reconstruction procedure. The function is unknown in the white region of the top left panel. In order to perform the extrapolation with another values of χ , the full procedure needs to be redone.

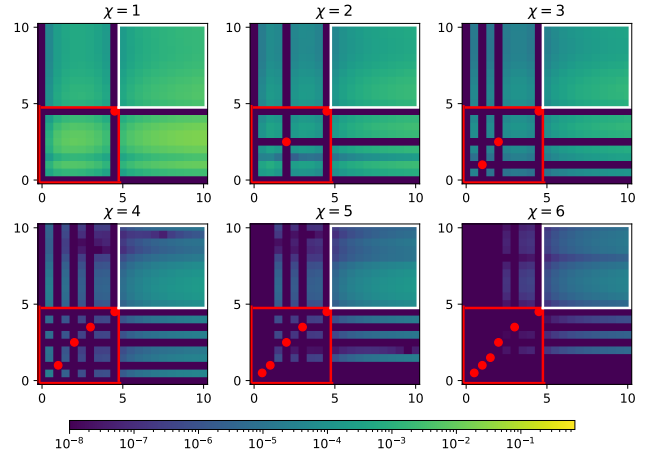


Figure 12. Error versus x and y at different stages of the L -shape Cross-Extrapolation. Same function as Fig.11. The pivots are only added inside the red square and we seek to extrapolate the function in the white square.

Appendix B: A remark on left and right currents.

The calculations shown in the main text correspond to the current $I^l(U, t)$ flowing from the left leads to the quantum dot. However, the current $I^r(U, t)$ flowing from the right lead is also available. In this appendix, we show that the additional information can be useful.

First, current conservation provides an independent non-trivial test of the accuracy of the cross-extrapolation. Current conservation reads,

$$\frac{dQ(U, t)}{dt} = I^l(U, t) + I^r(U, t) \equiv I_{\text{tot}}(U, t) \quad (\text{B1})$$

and indeed, this equality is true order by order,

$$\forall n, \quad \frac{dQ_n(U, t)}{dt} = I_n^l(U, t) + I_n^r(U, t) \quad (\text{B2})$$

so that where the series converges B1 is naturally satisfied; however an extrapolation may violate it. Figure 14 calculates both the right and left hand side of Eq.(B1) for $\alpha = \epsilon_d = V_b = 0$. We find that both extrapolations are in agreement within our calculated error bar, a non-trivial sanity check.

Second, just after the quench, the system experiments a transient current of electrons flowing out of the dot in order to reach the new stationary value of the charge Q . The currents I_l and I_r are very similar (identical for vanishing bias voltage $V_b = 0$). If one is interested in the asymptotic current $I = \lim_{t \rightarrow \infty} I_l(U, t) = -\lim_{t \rightarrow \infty} I_r(U, t)$, then it can be beneficial to extrapolate the difference $I^r - I^l$ that eliminates the short-time transient contribution and facilitate the extrapolation. We explore this idea in Fig.15 which shows I_r , $-I_l$ and the difference $(I^r - I^l)/2$ versus U ($t = 5$, panel a) and t ($U = 10$, panel b). We find that, indeed, the dynamics of $I^r - I^l$ shows less pronounced variations than the other two, yielding significantly smaller

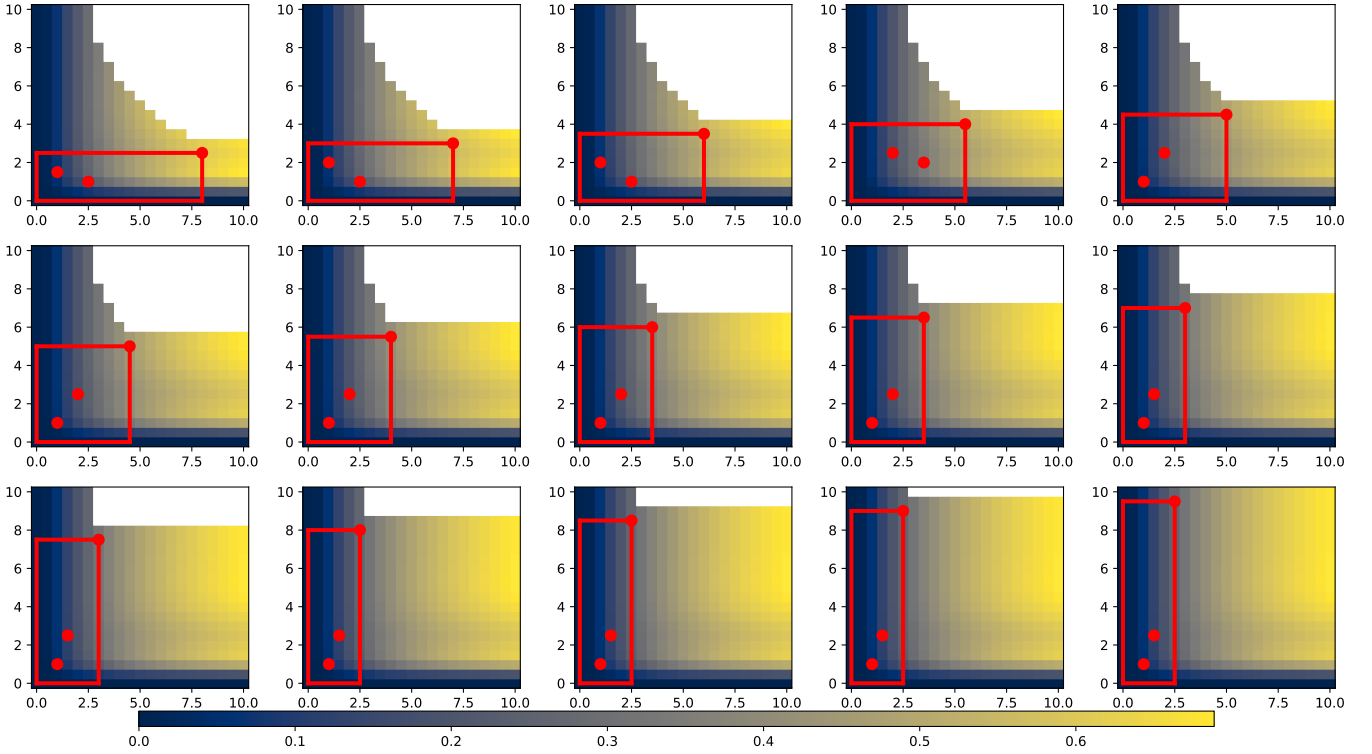


Figure 13. Extrapolated value of $f_{toy}(x, y)$ at different stages of the general-shape Cross-Extrapolation. Same function as Fig.11. The color map correspond to the values of f_{toy} known or extrapolated. Values in white (initially for $xy > 25$) are unknown and recovered performing the extrapolation line by line (the panels progress from left to right and then top to bottom). The pivots (red dots) are selected inside the red rectangle.

error bars in the extrapolation (roughly by a factor 5 in this example).

Appendix C: image reconstruction

In this appendix, we explore the possibility to use cross-extrapolation for image reconstruction, i.e. to recover a missing part of an image provided it exhibits a low-rank structure. We consider a black and white image of a clock which is represented by a 100×100 matrix M with $M_{ij} = 0$ (white pixel) and 1 (black pixel). The image is truncated and we use cross-extrapolation to try and recover the lost region. Figure 16 shows the extrapolation of the image for different values of the rank χ : while

not perfect, the reconstruction works reasonably well for $\chi = 35$ with 90% of the pixels reconstructed correctly.

Importantly, the error of the reconstruction can be monitored as well. For an extrapolated matrix M^χ , we use the norm-2 error per pixel

$$\epsilon_{\text{exact}} = \frac{1}{\sqrt{S}} \|M - M^\chi\|_2 = \frac{1}{\sqrt{S}} \left[\sum_{ij} |M_{ij} - M_{ij}^\chi|^2 \right]^{1/2} \quad (\text{C1})$$

to monitor the quality of the reconstruction and $\epsilon = \frac{1}{\sqrt{S}} \|M^\chi - M^{\chi+1}\|_2$ as our estimate of this error (S is the number of missing pixels). We find that our estimated error is in good agreement with the exact one.

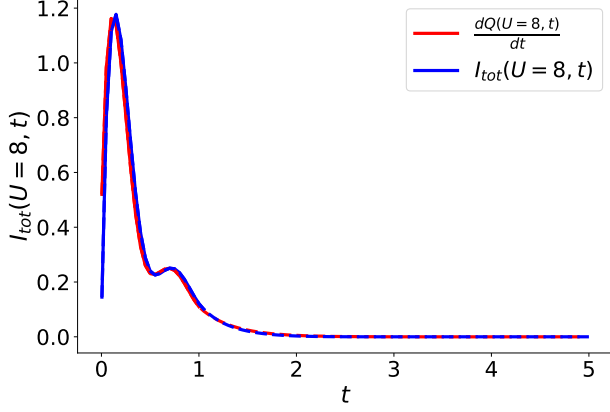


Figure 14. Current conservation for $\alpha = \epsilon_d = V_b = 0$, the derivative of the charge (in red) and the total current (sum of left and right current, in blue) at $U = 8$ as a function of time. Plane lines correspond to the simple summation and continue into dashed lines in the extrapolation regions. Both extrapolations are in good agreement and compatible with the predicted error bars.

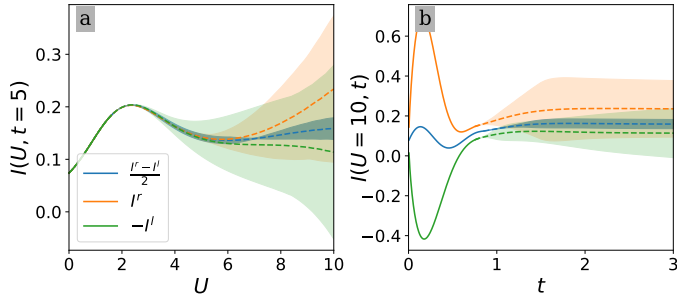


Figure 15. (a) Extrapolation of the difference of the right and left current divided by two (blue), the right current (orange) and the absolute value of the left current (green) using $\epsilon_d = -2$, $\alpha = 0$, and $V_b = 2$ at $t = 5$ as a function of U . Error bars are given by the colored area. (b) Same data for $U = 10$ as a function of time t .

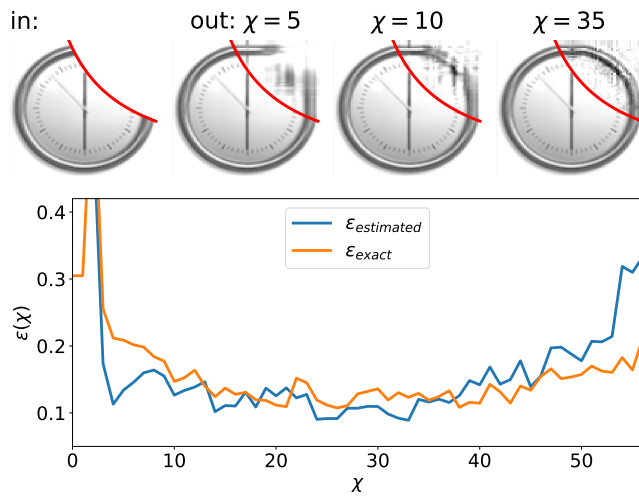


Figure 16. Top left: image of a clock, the part above the red lines has been cropped and needs to be recovered. Top right: image recovered using cross-extrapolation for three different values of $\chi = 5, 10$ and 35 . Bottom: estimated norm-2 error per pixel ϵ (blue) and exact norm-2 error ϵ_{exact} (orange) between the extrapolated matrix and the original one as a function of the rank. The optimal value of the rank is $\chi \approx 30$.